



Electrooxidation of ethylene glycol and glycerol by platinum-based binary and ternary nano-structured catalysts

Akinbayowa Falase, Michelle Main, Kristen Garcia, Alexey Serov, Carolin Lau, Plamen Atanassov*

Chemical & Nuclear Engineering Department, UNM Center for Emerging Energy Technologies, University of New Mexico, Albuquerque, NM 87131, USA

ARTICLE INFO

Article history:

Received 20 October 2011
Received in revised form 27 January 2012
Accepted 27 January 2012
Available online 4 February 2012

Keywords:

Electrocatalytic oxidations
Ethylene glycol
Glycerol
Fuel cells
Ternary catalyst

ABSTRACT

Spray pyrolysis of metal precursors was used to synthesize binary and ternary nano-structured Pt-based catalysts. Characterization of the catalysts was performed using SEM, TEM, and EDS to determine morphology, purity and composition. The electrochemical performance of synthesized Pt₈₄Ru₁₆, Pt₉₆Sn₄, and Pt₈₈Ru₆Sn₆ was evaluated via cyclic voltammetry and steady state polarization for oxidation of ethylene glycol and glycerol. The binary Pt₈₄Ru₁₆ and Pt₉₆Sn₄ catalysts had higher maximum currents and better stability than a templated Pt catalyst and templated ternary Pt₈₈Ru₆Sn₆ catalyst. All binary and ternary catalysts had less adsorbed reaction products during potential cycling than the templated platinum electrocatalyst. In situ infrared reflection absorption spectroscopy (IRRAS) analysis showed complete oxidation of ethylene glycol and glycerol with the binary and ternary catalysts by CO₂ generation. This work emphasizes the benefits provided by adding Ru and Sn to Pt catalysts for oxidation of complex alcohols.

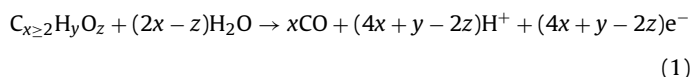
© 2012 Elsevier Ltd. All rights reserved.

1. Introduction

Ethylene glycol and glycerol have attracted interest in recent years as fuels for direct alcohol fuel cells (DAFCs). These fuels are advantageous compared to methanol due to their low toxicity, renewability from biomass, cost, and high energy density. Various groups have studied the reaction kinetics and feasibility of DAFCs based on these fuels in acid and alkaline media. Using an alcohol reduction catalyst synthesis process, Neto et al. showed that electrooxidation of ethylene glycol starts at lower potentials and current values increase with increasing ruthenium content, with similar effects with a PtSn/C catalyst [1]. Overall they discovered that PtSn/C electrocatalysts are better for ethylene glycol oxidation than PtRu/C catalysts due to oxidation at lower potentials and higher current values. Livshits, Peled and coworkers demonstrated the feasibility of a direct ethylene glycol fuel cell (DEGFC) by building a 10-cell stack with good performance in acid media with a nanoporous proton conducting membrane [2–5]. Chetty and Scott noted superior performance by a PtRuW ternary electrocatalyst compared to PtRu binary, and PtRuNi and PtRuPd ternary alloys [6]. While many of the reports concerning the feasibility of these fuel cells have dealt mostly with acid electrolytes, alkaline media presents many unique advantages for electrochemical reactions such as improvements in reaction kinetics at the anode

and cathode, and has thus been gaining interest in the literature [7–15].

Oxidation of these fuels in alkaline media is advantageous not only due to the improved kinetics of the reaction, and higher conversions [16,17]. The general reaction for oxidation of ethylene glycol and glycerol can be described by Eq. (1).



The reactions required for complete oxidation of ethylene glycol involves the liberation of 10 electrons while that of glycerol involve 14 electrons. Harvesting the maximum number of electrons is of utmost importance to utilize the fuel fully. Unfortunately, the complex oxidation reactions generate intermediates that can adsorb to and block the active sites of the catalyst, decreasing performance. Tin and ruthenium have been described in the literature as beneficial modifiers of platinum catalysts for biomass oxidation by helping to improve catalytic activity and decrease adsorbed oxidation intermediates [18–27]. Most reports discuss a bifunctional mechanism where the added metal provides oxygen species to aid in the removal of adsorbed CO and other incomplete oxidation products in acid and alkaline media. Coupling the benefits of an alkaline environment with the stability and reactivity improvements gained by using binary and possibly ternary catalysts presents a system in which the degree of fuel oxidation is maximized and catalyst poisoning is minimized.

* Corresponding author. Tel.: +1 505 277 2640; fax: +1 505 277 5433.
E-mail address: plamen@unm.edu (P. Atanassov).

We have synthesized, characterized, and electrochemically evaluated binary Pt₈₄Ru₁₆, and Pt₉₆Sn₄ catalysts, along with a ternary Pt₈₈Ru₆Sn₆ catalyst. The catalysts were synthesized using a spray pyrolysis approach that allows us to produce a nanostructured catalyst by etching away the monodisperse silica template [19,28,29]. This results in an “open frame” catalyst possessing improved transport and kinetic properties. Electrochemical characterization by cyclic voltammetry and steady state polarization revealed the performance improvements gained by alloying platinum with ruthenium and tin. We use infrared reflection absorption spectroscopy (IRRAS) to gain insight into the reaction kinetics on the surface and monitor oxidation products.

2. Experimental

2.1. Preparation of binary and ternary electrocatalysts via spray pyrolysis

Synthesis of templated nanostructured binary and ternary Pt alloys and a templated nanostructured Pt catalyst was achieved using spray pyrolysis. This procedure has been described previously, but we have performed the catalyst synthesis with modifications to the precursor material and reduction temperature [19,29]. Calculated amounts of platinum (IV) chloride, ruthenium (III) chloride hydrate, and/or tin (II) chloride hydrate [Sigma–Aldrich Co.], with 20 nm monodisperse Ludox[®] TM50 colloidal silica [Sigma–Aldrich Co.] were mixed as a precursor solution in 30 mL of de-ionized water. Concentrated hydrochloric acid was added drop-wise while stirring until the precursors dissolved. The dissolved precursor solution was atomized and dried through a furnace at 125 °C using N₂ as the carrier gas. A standard humidifier was modified in order to expose the ultrasonic membrane. The catalyst precursor solution was then positioned on top of the membrane in order to generate the aerosol. All catalysts were made as 20 wt.% catalyst on silica template.

Pyrolyzed particles were collected on 0.2 μm filter paper, and alloys were formed by reduction of the oxide powders under 5% H₂ in N₂ at 500 °C for 2 h with a ramp rate of 1 °C/min and at a total gas flow rate of 100 mL/min. The silica template was then etched in a 7 M KOH solution for 72 h. Afterwards, the solution was filtered and washed 3× with DI water to remove the KOH. The collected catalyst was then dried in an oven at 80 °C.

2.2. Physical characterization

Following reduction and etching the silica template from the catalysts, morphology, purity, and composition of the synthesized powders were determined using scanning electron microscopy (SEM), transmission electron microscopy (TEM), and energy dispersion spectroscopy (EDS). SEM and TEM provided information on the morphology of the bulk and individual particles of the catalysts while EDS was used to determine the composition of the samples and compare to the starting solution.

Surface areas were measured by the N₂-BET method using a Micromeritics 2360 Gemini Analyzer. Scanning electron microscopy (SEM) was performed using a Hitachi S-5200 Nano SEM with an accelerating voltage of 10 keV. Transmission electron microscopy (TEM) was performed using a JEOL 2010 instrument with an accelerating voltage of 200 keV. Powdered samples were analyzed by X-ray diffraction (XRD) using a Scintag Pad V diffractometer (Bragg-Brentano geometry) with DataScan 4 software (from MDI, Inc.) for system automation and data collection. Cu KR radiation (40 kV, 35 mA) was used with a Bicron Scintillation detector (with a pyrolytic graphite curved crystal monochromator). Data were analyzed with Match! 1.11 Software (Crystal Impact) using the ICDD

(International Center for Diffraction Data) PDF4 data-base (rev. 2009) for phase identification. Various catalyst compositions were synthesized and screened based on reports of similar catalysts in the literature. The best performing catalysts in each group are presented.

2.3. Electrochemical and in situ infrared characterization

A 5 μL aliquot of a 3 mg/mL catalyst ink composed of 5 wt.% Nafion, and de-ionized water with isopropyl alcohol in a 4:1 ratio was deposited on polished glassy carbon electrodes with a 5 mm outer diameter for a final catalyst loading of 76 μg/cm². The electrodes were allowed to air dry for 30 min.

Cyclic voltammetry was conducted in 1.0 M KOH at room temperature. When required, glycerol and ethylene glycol were added to the electrolyte to make 0.1 M solutions. A Pt mesh and Hg/HgO electrode [XR-440 Radiometer Analytical SAS] were used as counter and reference electrodes, respectively. Before each experiment, the electrolyte solution was deoxygenated by bubbling N₂ gas for at least 15 min. Polarization curves were constructed by averaging the last 10% of points (90 points) during each 15-min step in potentiostatic mode with step increments of 25 mV. All potentials in this discussion are referred to the reversible hydrogen electrode (RHE) scale.

In situ infrared reflection adsorption spectroscopy (IRRAS) experiments were performed at room temperature with a Nicolet 6700 FT-IR spectrometer equipped with a Mercury Cadmium Telluride (MCT) detector cooled with liquid nitrogen. Experimental setup is described previously [30–32]. For each spectra, 128 interferograms were added together to each spectrum at a resolution of 8 cm⁻¹ with unpolarized light. Absorbance units of the spectra are defined as $A = -\log(R/R_0)$, where R and R_0 represent reflected IR intensities corresponding to the sample and reference single beam spectrum, respectively. Thus, a positive peak in the resulting spectrum indicates a production of species, while a negative peak indicates consumption or decrease in concentration of a species compared to the reference spectrum. The reference spectrum was collected at 0.140 V (RHE) vs. an Ag/AgCl reference electrode in 1.5 mL of 0.1 M respective fuel (ethylene glycol or glycerol) and 0.1 M KOH, using linear sweep voltammetry with a scan rate of 1 mV/s from 0.140 V to 1.18 V (RHE). A thin layer of ink was pipetted onto a polished glassy carbon electrode with a diameter of 5 mm. A ZnSe hemisphere was used as the IR window, and the working electrode was pressed against the window, creating a thin solution layer with a thickness of a few micrometers. The incident angle of the IR radiation passing through the ZnSe window was 36° [30]. Argon was used to purge the electrolyte while dry air was used to purge the spectrometer and chamber, reducing the spectral interference from CO₂ and water vapor.

3. Results and discussion

3.1. Characterization of electrocatalysts

Spray pyrolysis of templated catalysts is a powerful synthesis tool due to the degree of control granted over the final catalyst composition due to each individual aerosol droplet having the same composition as the precursor solution. SEM micrographs show the droplet and porous “sponge-like” morphology (Fig. 1A and B), as expected from the templating procedure. The removal of the silica nanoparticles leaves pores in the catalytic structure that increases catalyst utilization, even though the surface area is lower than catalysts supported on high surface area materials such as carbon. Catalyst compositions and BET surface area are described in Table 1.

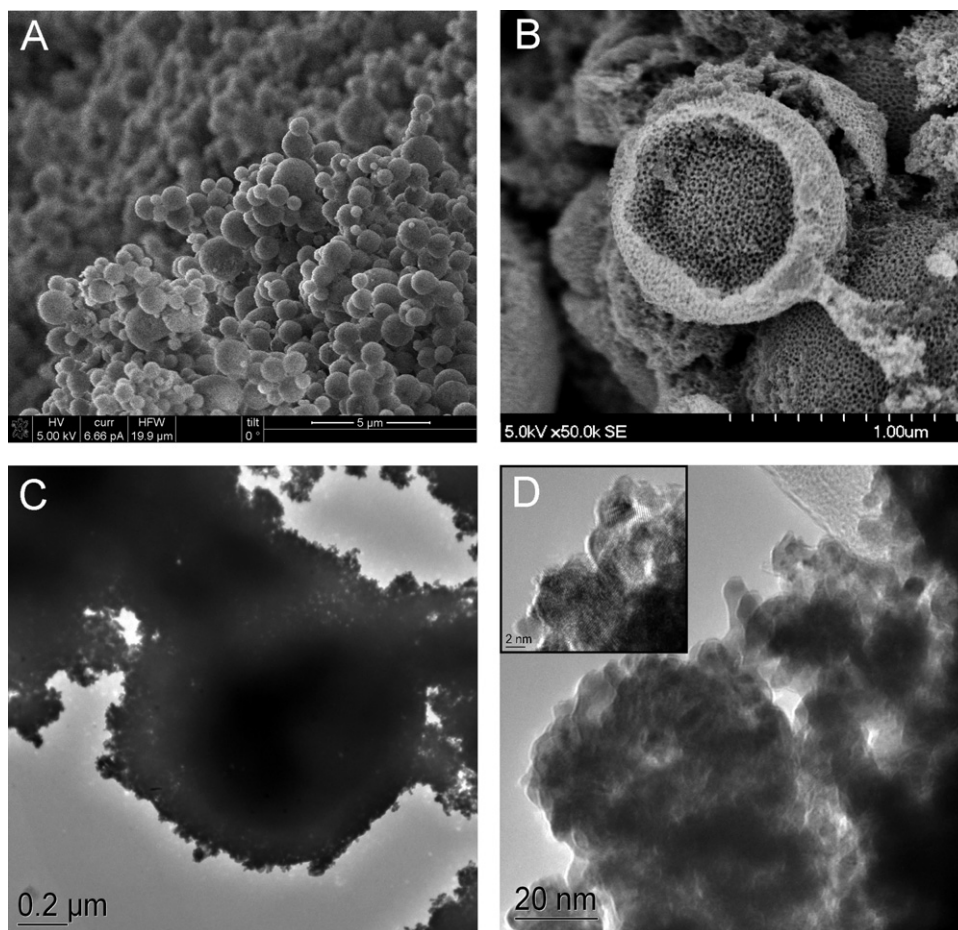


Fig. 1. SEM and TEM micrographs of $\text{Pt}_{88}\text{Ru}_6\text{Sn}_6$ catalyst. Images of the unetched (A) and etched (B) catalyst show the droplet-like morphology of each individual catalyst particle. The templated morphology extends through the interior of the particle as shown in the SEM (B) and TEM (C and D) micrographs. The high resolution image (D, insert) shows lattice fringes from the Pt, Ru, and Sn catalyst.

TEM micrographs show the void spaces in the pores of the catalyst as well as the individual grains of the catalytic particles (Fig. 1C, D, D insert). Grain sizes of the particles were 5–15 nm.

Catalyst morphology, particle size and distribution are dependent on synthesis procedures. The spray pyrolysis procedure can be performed with an atomizer, producing particles with a narrower size distribution than those produced here with a modified humidifier serving as the aerosol generator [33,34].

XRD patterns of the synthesized Pt, PtRu, PtSn, and PtRuSn catalysts are shown in Fig. 2. Phase planes of the platinum appear at the corresponding angles from (1 1 1), (2 0 0), (2 2 0), (3 1 1), and (2 2 2) phases. There were no diffraction peaks associated with separated ruthenium, tin or their oxide species detected from the XRD measurements. The peaks are shifted slightly compared to one another possibly due to incorporation of ruthenium or tin into the platinum crystal lattice. The nanostructured Pt catalyst is also slightly shifted from the dashed lines, but this could be due to the instrument itself because no impurities were detected by EDS during SEM or TEM analysis.

Table 1
Pt based nanostructured catalyst compositions and surface areas.

Catalyst name	Expected composition	Composition (± 2)	BET surface area (m^2/g)
Pt(nanostructured)	100	100	27
$\text{Pt}_{84}\text{Ru}_{16}$	85:15	84:16	27
$\text{Pt}_{96}\text{Sn}_4$	95:5	96:4	27
$\text{Pt}_{88}\text{Ru}_6\text{Sn}_6$	90:5:5	88:6:6	33

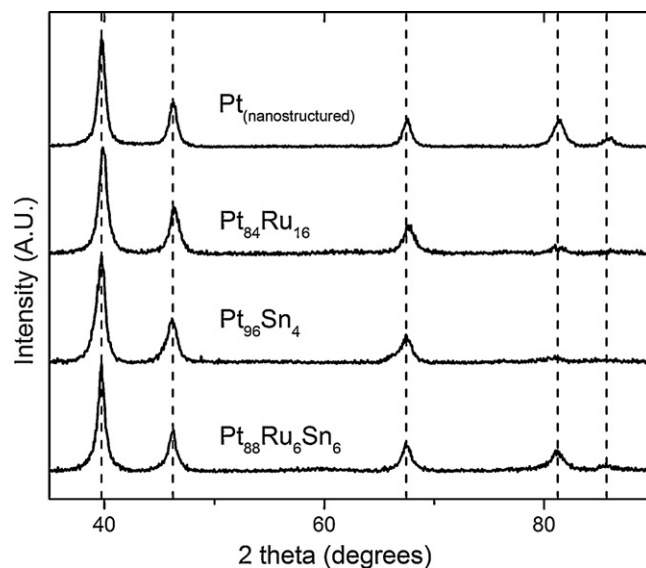


Fig. 2. XRD diffraction patterns of synthesized nanostructured Pt and Pt based catalysts over the scan range of 2–90° (35–90° shown for clarity). The dashed lines represent the typical diffraction angles of the *fcc* phase of Pt.

3.2. Electrochemical studies of binary and ternary catalysts for ethylene glycol and glycerol oxidation

The synthesized binary and ternary catalysts were tested as electrocatalysts for the anodic oxidation of ethylene glycol and were compared to a synthesized spray pyrolyzed nanostructured platinum catalyst. Cyclic voltammetry was used to evaluate the performance of the electrocatalysts for the oxidation of each fuel. The catalysts were cycled through the potential range multiple times until a steady state value was reached (cycle 4 for all catalysts presented here). The performance of each catalyst is presented in Fig. 3.

The voltammograms exhibit expected behavior previously described regarding oxidation of these fuels in alkaline media [35,36]. There are two oxidation peaks in the forward scan direction and one in the reverse direction. The singular anodic peak in the negative sweep represents oxidation of incompletely oxidized carbonaceous intermediates on the surface of the catalysts left over from the positive sweep [37,38]. Accumulation of these adsorbed products block active sites on the catalyst, decreasing performance. Roquet et al. speculated that since the first oxidation wave of glycerol occurs in the platinum oxidation region, glycerol oxidation requires the presence of adsorbed hydroxyls on the surface [39]. They also speculated that because the forward and reverse sweep oxidative curves are not aligned, there is a limiting rate of glycerol adsorption on the reduced platinum surface. Since the profiles for ethylene glycol and glycerol oxidation are similar, we believe that this explanation is suitable for oxidation of both fuels.

The recorded current is normalized to the BET surface area (Table 1) of the catalysts in order to determine metal utilization. In terms of maximum peak current, the binary Pt₈₄Ru₁₆ catalyst showed enhanced oxidation behavior for both ethylene glycol oxidation and glycerol oxidation (Fig. 3), followed by the nanostructured Pt. The Pt₉₆Sn₄ had higher oxidative currents than the Pt₈₈Ru₆Sn₆ catalyst, but both performed worse than the Pt₈₄Ru₁₆ and nanostructured Pt catalysts. When oxidizing ethylene glycol, the nanostructured Pt catalyst exhibits 3 distinct features. There is a shoulder at 0.704V, the peak at 0.747V, and a softer shoulder at 0.826V. Possible shoulders for the binary and the broad oxidative peaks that they exhibit obscure ternary catalysts. Although glycerol has more electrons to transfer during complete oxidation, more maximum current is achieved while oxidizing ethylene glycol compared to glycerol due to a less complex oxidative pathway. A summary of the catalyst performance is given in Table 2. The catalysts were evaluated in terms of their onset potential, the peak potentials, current densities, and the ratio of forward anodic peak to reverse peak current. The trend of the onset potential for ethylene glycol oxidation was PtRu > PtSn > Pt (nanostructured) > PtRuSn (in terms of greatest performance; meaning lowest onset potential) while for glycerol oxidation the trend was PtRu > PtSn > PtRuSn > Pt (nanostructured). For both fuels the binary catalysts had the lowest onset potentials. The binary PtRu catalyst

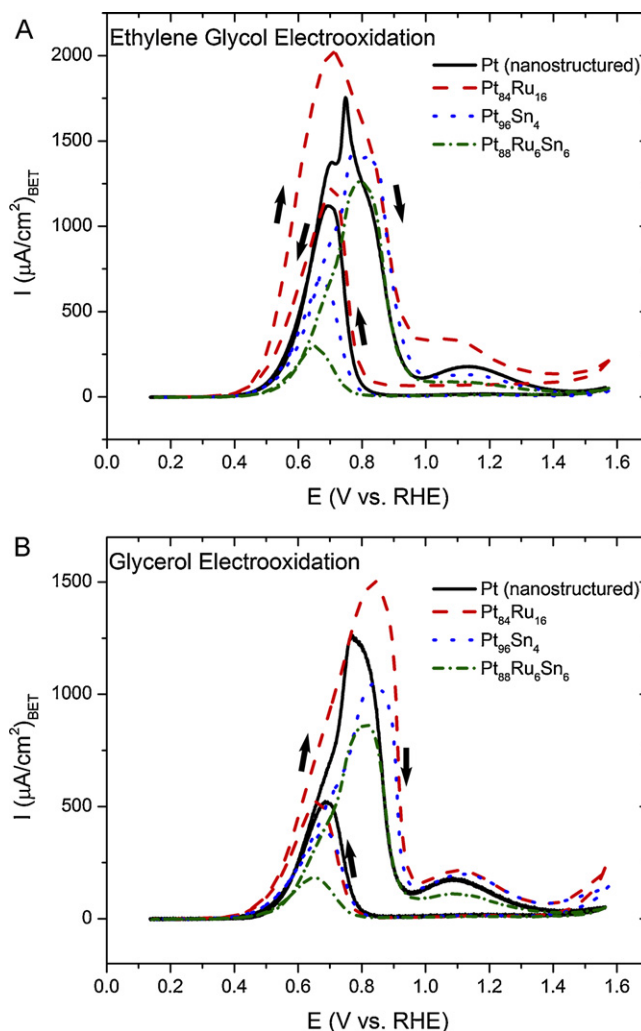


Fig. 3. Cyclic voltammograms of Pt, Pt₈₄Ru₁₆, Pt₉₆Sn₄, and Pt₈₈Ru₆Sn₆ catalysts vs. ethylene glycol (A) and glycerol (B). Each catalyst was cycled until a steady state was reached at 10 mV/s in 1.0 M KOH electrolyte with 0.1 M ethylene glycol and glycerol, respectively. The current density was calculated with respect to the BET surface area.

had the lowest oxidative peak potential, and the highest current for both ethylene glycol and glycerol oxidation. For both fuels, the ternary PtRuSn electrocatalyst performed poorly compared to the binary and nanostructured Pt catalyst. From these results it seems that alloying platinum specifically with both ruthenium and tin simultaneously as a ternary catalyst is not beneficial in terms of achieving the maximum current compared to binary PtRu and PtSn catalysts. The binary and ternary electrocatalysts have

Table 2
Comparison of catalyst performance for ethylene glycol and glycerol electrooxidation.

Catalyst	E_{onset} (V)	E_F (V)	I_F ($\mu\text{A}/\text{cm}^2_{\text{BET}}$)	E_R (V)	I_R ($\mu\text{A}/\text{cm}^2_{\text{BET}}$)	I_F/I_R
Ethylene glycol						
Pt(nanostructured)	0.36	0.76	1718.52	0.69	1117.47	1.54
Pt ₈₄ Ru ₁₆	0.29	0.72	2109.55	0.69	1271.58	1.66
Pt ₉₆ Sn ₄	0.35	0.78	1408.29	0.67	691.21	2.04
Pt ₈₈ Ru ₆ Sn ₆	0.38	0.80	1260.27	0.64	295.05	4.27
Glycerol						
Pt(nanostructured)	0.40	0.79	1245.21	0.68	514.86	2.42
Pt ₈₄ Ru ₁₆	0.33	0.85	1568.50	0.65	542.41	2.89
Pt ₉₆ Sn ₄	0.34	0.85	1044.91	0.67	378.80	2.76
Pt ₈₈ Ru ₆ Sn ₆	0.36	0.82	862.79	0.64	183.30	4.71

E_{onset} : onset potential (vs. RHE); E_F , I_F : peak potential and current density, respectively, of main oxidation peak at 10 mV/s (vs. RHE); E_R , I_R : peak potential and current density, respectively, of reverse oxidation peak at 10 mV/s (vs. RHE); I_F/I_R : ratio of forward main and reverse oxidation peak current density.

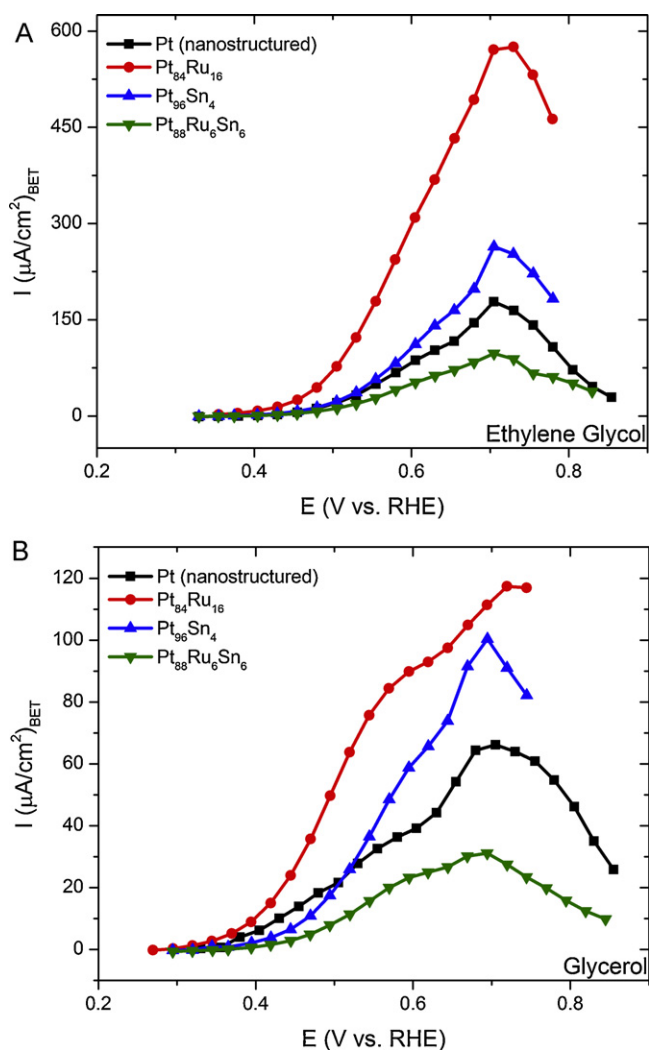


Fig. 4. Steady-state polarization curves of Pt₈₄Ru₁₆, Pt₈₈Ru₆Sn₆, and Pt₉₆Sn₄ catalysts vs. ethylene glycol (top) and glycerol (bottom). 1.0 M KOH electrolyte with 0.1 M ethylene glycol and glycerol, respectively. The current density was calculated with respect to the BET surface area.

higher I_F/I_R ratios than the nanostructured Pt catalyst, signaling that accumulation of oxidation residues during the catalytic processes is less than on the pure Pt catalyst and similar catalysts reported in acidic media [40]. The ternary catalyst had the highest I_F/I_R ratio, suggesting that the effects of the modifier tin and ruthenium atoms help to prevent buildup of oxidation products on the platinum active sites, even though its oxidative performance lacked that of binary and nanostructured Pt catalysts. Steady-state polarization curves of ethylene glycol and glycerol oxidation on the catalyst were obtained under potentiostatic conditions (Fig. 4). Maximum currents for the PtRu catalyst were higher than the PtRu and PtRuSn catalysts for both ethylene glycol and glycerol oxidation. For ethylene glycol electrooxidation, the maximum current achieved by the PtRu catalyst was twice that of the PtSn, 3.2 times that of the nanostructured platinum catalyst and 6 times that of the ternary PtRuSn catalyst following a trend of PtRu > PtSn > Pt (nanostructured) > PtRuSn. Similar performance was seen with glycerol. The maximum current for the PtRu electrocatalyst was 1.2 times higher than the PtSn, 1.77 times that of the platinum, and 3.7 times higher than the PtRuSn. At potentials lower than 0.51 V, the Pt catalyst has a higher current than the binary PtSn catalyst, but at higher potentials the PtSn catalyst outperforms the Pt catalyst. The trend for catalyst performance during glycerol oxidation trends

Table 3

Infrared frequencies observed by in situ FTIR spectroscopy of oxidation products formed during EG and Gly electrooxidation.

Wavenumber (cm ⁻¹)	Assignment
1004	Alcohol CH ₂ -OH stretch [44]
1071	Aldehyde stretch (glyoxal, glycolate, glyceraldehyde) [36,42–44]
1094	Alcohol stretching [44]
1111	CH-OH stretch [44]
1236	C-O stretch of glycolate [45]
1303	Symmetric -OOC-COO ⁻ , glyceraldehyde [42,46]
1320	Symmetric COO ⁻ stretch of glycolate, oxalate [43,45]
1353	Adsorbed carbonylate [45]
~1405	Carbonate CO ₃ ²⁻ [42,45]
1445, 1548, 1630	Carboxylate groups [47]
1574	Asymmetric -OOC-COO ⁻ [42]
~1589	H-O-H deformation of adsorbed water, asymmetric COO ⁻ stretch of glyoxal, glycolate, glyoxylate [43]
~1665	Carbonyl and carboxyl stretches [47]
1723	Carboxyl stretching [47]
2343	CO ₂ asymmetric stretch

as PtRu > PtSn > Pt (nanostructured) > PtRuSn at potentials higher than 0.51 V.

3.3. IRRAS characterization of ethylene glycol and glycerol oxidation

The oxidation pathway of ethylene glycol has been described previously [41,42]. This reaction scheme consists of a complex parallel 2-electron steps oxidation mechanism first from ethylene glycol to glycolaldehyde. The molecule is then oxidized to either glyoxal or glycolic acid, then to glyoxylic acid followed by oxalic acid and then finally CO₂. It is worth noting that oxalic acid is in the [A²⁻] deprotonated state due to its relatively low pK_a values of 1.38 and 4.28.

Infrared spectroscopy was used to elucidate the ethylene glycol electrooxidation reaction mechanism on the binary and ternary catalysts. Each spectrum was recorded in 0.1 M potassium hydroxide solution with 0.1 M of ethylene glycol or glycerol. Some major band frequencies are summarized in Table 3 for ethylene glycol and glycerol oxidation. Glycolaldehyde is not present in the table due to dimerization in neutral media that is further complicated in alkaline solution [43] (Fig. 5).

The oxidation pathway and kinetics as shown via infrared spectra for ethylene glycol oxidation are very similar for the binary and ternary catalysts. The peaks for alcohol stretching at 1000 cm⁻¹, aldehyde stretching at 1070 cm⁻¹ indicative of glyoxal and glycolate species, symmetric COO⁻ stretching at 1320 cm⁻¹, and asymmetric -OOC-COO⁻ stretching at 1574 cm⁻¹ indicate the presence of glyoxal and glycolate at 0.5 V for the PtRu catalyst, and 0.61 V for the PtSn and PtRuSn catalyst. Asymmetric COO⁻ stretching along with water deformation results in a very strong peak at 1589 cm⁻¹. Carbonate formation at 1405 cm⁻¹ begins between 0.4 and 0.5 V, and increases up to 0.6 V where it seems to remain steady or decrease as Demarconnay et al. observed [45]. A small peak due to bridge bonded CO species at 1856 and 1813 cm⁻¹ with the much smaller corresponding linear CO peak at 2000 cm⁻¹ appears at 0.28 V for the PtSn and PtRuSn catalysts, and at 0.61 V for the PtRu catalyst [48,49]. These peaks grow slightly in intensity as the electrode becomes more polarized. As the reaction progresses, CO₂ begins to form at 0.73 V for the PtRu catalyst [45], and 0.84 V for the PtSn and PtRuSn catalysts. Production of a carboxylic acid evident by absorbance bands at 1723 cm⁻¹ 1236 cm⁻¹ and 1095 cm⁻¹ is enhanced on the Pt₈₄Ru₁₆ catalyst at high (1.18 V) potentials compared to the PtSn and PtRuSn catalyst.

The electrooxidation pathway of glycerol has been described recently in alkaline media. Kwon et al. used high performance liquid

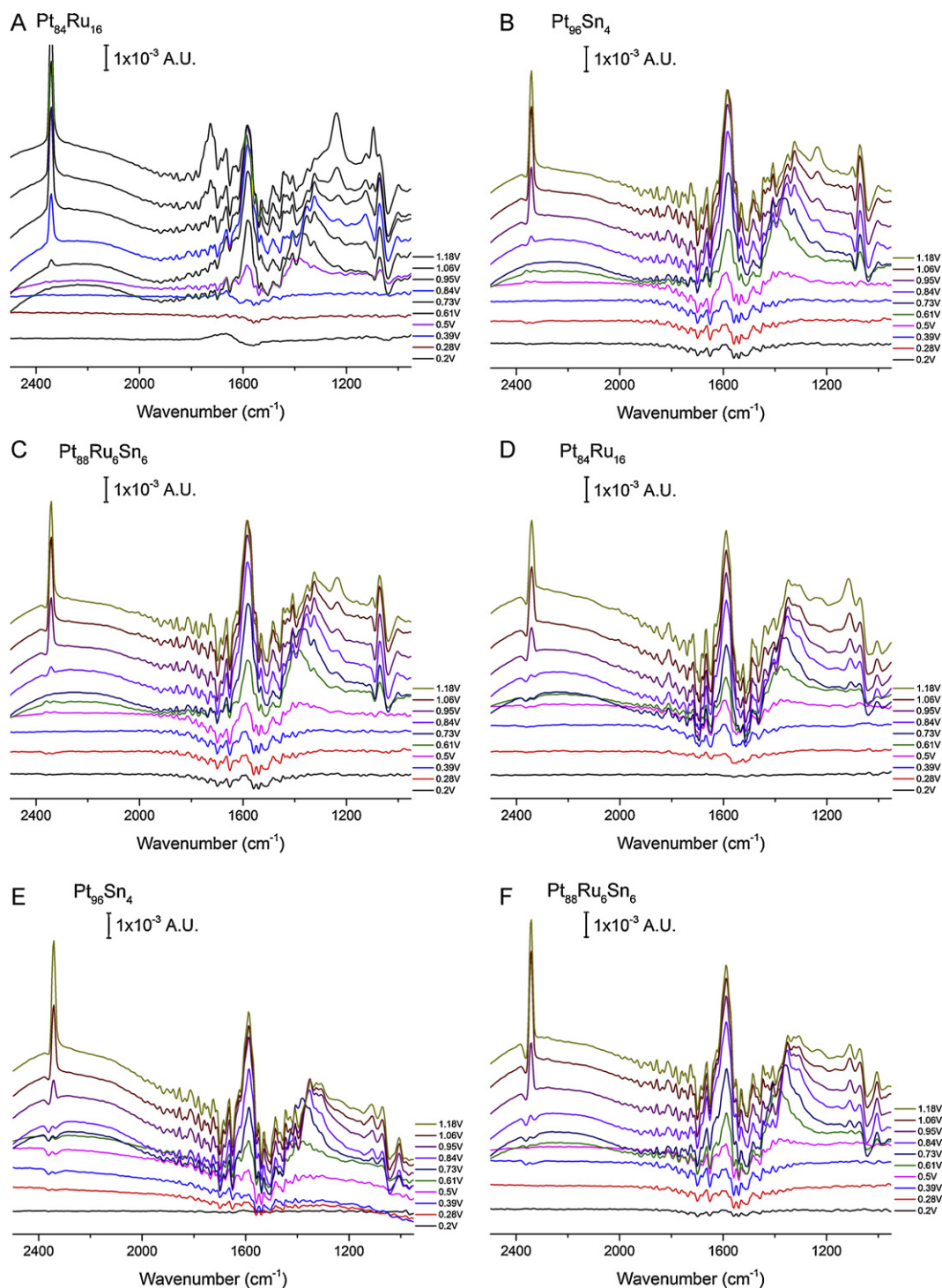


Fig. 5. IRRAS spectra of ethylene glycol (A–C) and glycerol (D–F) oxidation on binary and ternary Pt-based catalysts. 1 mV/s scan rate in 0.1 M KOH and 0.1 M fuel.

chromatography coupled with online electrochemical mass spectroscopy to elucidate the complex oxidation reaction scheme on gold and platinum catalysts [16]. They found high concentrations of glyceraldehyde to be the first oxidation product at 0.4 V, followed by glyceric acid. Dihydroxyacetone, hydroxypyruvic acid, glycolic acid, formic acid, oxalic acid, and tartronic acid were detected at low concentrations.

The oxidation reaction pathway of glycerol on the binary and ternary Pt based catalysts was similar amongst the catalysts.

Absorbance bands at 1070 cm^{-1} corresponding to aldehydes appear at 0.61 V and grow in intensity as the potential increases. As with ethylene glycol, a strong peak at 1589 cm^{-1} results from the water stretching and carboxylic acids that absorb at the same wavelength. A small peak due to bridge bonded CO species at 1856 and 1813 cm^{-1} with the even smaller corresponding linear CO peak at 2000 cm^{-1} appears at 0.28 V and grows slightly in intensity as the electrode becomes more polarized. CO_2 formation begins at 0.84 V for all three catalysts.

4. Conclusions

We have reported the synthesis and characterization of binary and ternary templated catalysts synthesized by spray pyrolysis. The use of spray pyrolysis was chosen due to its ease of creating templated catalysts with desired composition. EDS analysis confirmed the composition of the as-created catalysts. The catalysts had an open frame sponge like morphology caused by template removal via etching of the silica catalyst. Cyclic voltammetry and steady state polarization showed that the binary Pt₈₄Ru₁₆ had both higher oxidative currents and better catalytic stability vs. nanostructured platinum, binary PtSn, and ternary PtRuSn catalysts. The ratio of forward peak current to reverse peak current was high, indicating that accumulation of oxidation products on the catalyst surface is not as significant as it is for reactions using similar catalysts in acid media. The addition of both ruthenium and tin modifiers to platinum catalysts is not beneficial for maximum current generation, as seen in the cyclic voltammetry and steady state polarization experiments, but adsorption of reaction intermediates that can block the electrode and decrease performance is lower on the ternary catalysts than the binary PtRu, PtSn and nanostructured Pt catalyst. Both the binary and ternary electrocatalysts are capable of complete oxidation of both ethylene glycol and glycerol via the presence of CO₂ as shown by in situ IRRAS. This work demonstrates the complimentary effect of Ru and Sn modifiers in a binary platinum based catalyst to achieve higher catalyst performance for the electrooxidation of ethylene glycol and glycerol.

Acknowledgments

The authors would like to thank Dr. Andrew De La Riva for assistance with the TEM images, and Dr. Barr Halevi, Eric Peterson, and Dr. Rosalba Rincon for assistance in obtaining XRD data. Work was supported in part by the DOE EPSCoR NM Implementation Award. Akinbayowa Falase is thankful for support from the Louis Stokes Alliance for Minority Participation (LSAMP) Bridge to the Doctorate VII HRD #0832947 program.

References

- [1] A. Neto, T. Vasconcelos, R. Da Silva, M. Linardi, E. Spinace, *J. Appl. Electrochem.* 35 (2005) 193.
- [2] V. Livshits, M. Philosoph, E. Peled, *J. Power Sources* 178 (2008) 687.
- [3] V. Livshits, E. Peled, *J. Power Sources* 161 (2006) 1187.
- [4] E. Peled, V. Livshits, T. Duvdevani, *J. Power Sources* 106 (2002) 245.
- [5] E. Peled, T. Duvdevani, A. Aharon, A. Melman, *Electrochim. Solid State Lett.* 4 (2001) A38.
- [6] R. Chetty, K. Scott, *J. Appl. Electrochem.* 37 (2007) 1077.
- [7] K. Matsuoka, Y. Iriyama, T. Abe, M. Matsuoka, Z. Ogumi, *J. Power Sources* 150 (2005) 27.
- [8] M. Abdel Rahim, R. Abdel Hameed, M. Khalil, *J. Power Sources* 134 (2004) 160.
- [9] L. Jiang, A. Hsu, D. Chu, R. Chen, *Int. J. Hydrogen Energy* 35 (2010) 365.
- [10] C. Xu, P. Shen, Y. Liu, *J. Power Sources* 164 (2007) 527.
- [11] Y. Feng, W. Yin, Z. Li, C. Huang, Y. Wang, *Electrochim. Acta* 55 (2010) 6991.
- [12] A. Verma, S. Basu, *J. Fuel Cell Sci. Technol.* 2 (2005) 234.
- [13] C. Bianchini, P.K. Shen, *Chem. Rev.* 109 (2009) 4183.
- [14] J. Varcoe, R. Slade, *Fuel Cells* 5 (2005) 187.
- [15] A. Serov, C. Kwak, *Appl. Catal. B: Environ.* 97 (2010) 1.
- [16] Y. Kwon, K.J.P. Schouten, M.T.M. Koper, *Chemcatchem* 3 (2011) 1176.
- [17] E. Antolini, E.R. Gonzalez, *J. Power Sources* 195 (2010) 3431.
- [18] M. Watanabe, S. Motoo, *J. Electroanal. Chem.* 60 (1975) 267.
- [19] E.E. Switzer, T. Olson, A. Datye, P.B. Atanassov, M. Hibbs, C. Cornelius, *Electrochim. Acta* 54 (2009) 989.
- [20] M. Watanabe, M. Uchida, *J. Electroanal. Chem.* 229 (1987) 395.
- [21] A. Deffernez, S. Hermans, M. Devillers, *Appl. Catal. A: Gen.* 282 (2005) 303.
- [22] Y.H. Chu, Y.G. Shul, *Int. J. Hydrogen Energy* 35 (2010) 11261.
- [23] A. Oliveira Neto, R.R. Dias, M.M. Tusi, M. Linardi, E.V. Spinace, *J. Power Sources* 166 (2007) 87.
- [24] C. Lamy, E. Belgsir, J. Leger, *J. Appl. Electrochem.* 31 (2001) 799.
- [25] F. Delime, J.-M. Leger, C. Lamy, *J. Appl. Electrochem.* 29 (1999) 1249.
- [26] Z. Jusys, T. Schmidt, L. Dubau, K. Lasch, L. Jorissen, J. Garche, R. Behm, *J. Power Sources* 105 (2002) 297.
- [27] T. Kawaguchi, Y. Rachi, W. Sugimoto, Y. Murakami, Y. Takasu, *J. Appl. Electrochem.* 36 (2006) 1117.
- [28] Y. Lu, H. Fan, A. Stump, T. Ward, T. Rieker, C. Brinker, *Nature* 398 (1999) 223.
- [29] E.E. Switzer, A.K. Datye, P.B. Atanassov, *Top. Catal.* 46 (2007) 334.
- [30] P. Faguy, N. Marinkovic, *Appl. Spectrosc.* 50 (1996) 394.
- [31] D.A. Konopka, M. Li, K. Artyushkova, N. Marinkovic, K. Sasaki, R. Adzic, T.L. Ward, P.B. Atanassov, *J. Phys. Chem. C* 115 (2011) 3043.
- [32] A. Kowal, M. Li, M. Shao, K. Sasaki, M.B. Vukmirovic, J. Zhang, N.S. Marinkovic, P. Liu, A.I. Frenkel, R. Adzic, *Nat. Mater.* 8 (2009) 325.
- [33] S.B. Rathod, T.L. Ward, *J. Mater. Chem.* 17 (2007) 2329.
- [34] M.T. Bore, S.B. Rathod, T.L. Ward, A.K. Datye, *Langmuir* 19 (2003) 256.
- [35] P. Shen, C. Xu, *Electrochim. Commun.* 8 (2006) 184.
- [36] P. Christensen, A. Hamnett, *J. Electroanal. Chem.* 260 (1989) 347.
- [37] J.H. Kim, S.M. Choi, S.H. Nam, M.H. Seo, S.H. Choi, W.B. Kim, *Appl. Catal. B: Environ.* 82 (2008) 89.
- [38] G. Girishkumar, T.D. Hall, K. Vinodgopal, P.V. Kamat, *J. Phys. Chem. B* 110 (2006) 107.
- [39] L. Roquet, E. Belgsir, J. Leger, C. Lamy, *Electrochim. Acta* 39 (1994) 2387.
- [40] H.J. Kim, S.M. Choi, S. Green, G.A. Tompsett, S.H. Lee, G.W. Huber, W.B. Kim, *Appl. Catal. B: Environ.* 101 (2011) 366.
- [41] B. Wieland, J.P. Lancaster, C.S. Hoaglund, P. Holota, W.J. Tornquist, *Langmuir* 12 (1996) 2594.
- [42] L. Wang, H. Meng, P.K. Shen, C. Bianchini, F. Vizza, Z. Wei, *Phys. Chem. Chem. Phys.* 13 (2011) 2667.
- [43] S. Chang, Y. Ho, M. Weaver, *J. Am. Chem. Soc.* 113 (1991) 9506.
- [44] D.R. Lide, *CRC Handbook of Chemistry and Physics: A Ready-reference Book of Chemical and Physical Data*, CRC Press, 2004.
- [45] L. Demarconnay, S. Brimaud, C. Coutanceau, J.-M. Leger, *J. Electroanal. Chem.* 601 (2007) 169.
- [46] M. Simões, S. Baranton, *Appl. Catal. B: Environ.* (2011).
- [47] M. Avramov-Ivic, J. Leger, B. Beden, F. Hahn, C. Lamy, *J. Electroanal. Chem.* 351 (1993) 285.
- [48] M. Koper, T. Shubina, R. van Santen, *J. Phys. Chem. B* 106 (2002) 686.
- [49] C. Korzeniewski, *Crit. Rev. Anal. Chem.* 27 (1997) 81.